Available online at www.sciencedirect.com
ScienceDirect
Trans. Nonferrous Met. Soc. China 25(2015) 191−198
Transactions of Nonferrous Metals Society of China
www.tnmsc.cn

Oxidation and hot corrosion of electrodeposited Ni−7Cr−4Al nanocomposite

Hai-jun ZHANG, Jian-feng SUN

College of Materials Science and Engineering, Heilongjiang University of Science and Technology, Harbin 150022, China

Received 28 November 2013; accepted 7 April 2014

Abstract: A Ni−7Cr−4Al (mass fraction, %) nanocomposite was fabricated by co-electrodeposition of Ni with Cr (40 nm) and Al (100 nm) nanoparticles from a nickel sulfate bath, and its oxidation at 800 °C in air and hot corrosion under molten 75% Na_2SO_4 + 25% NaCl salts (mass fraction) at 750 °C were investigated. For comparison, Ni−11Cr nanocomposite and Ni-film were also investigated in order to elucidate the effect of Cr nanoparticles. The results indicate that Cr and Al nanoparticles are dispersed in the electrodeposited nanocrystalline Ni grains (in size range of 20−60 nm). Ni−7Cr−4Al nanocomposite exhibits a dramatically increased oxidation resistance compared with Ni−11Cr nanocomposite and Ni-film due to the fast formation of alumina scale, which also improves its hot corrosion resistance under molten 75% Na_2SO_4 + 25% NaCl salts.

Key words: Ni−Cr−Al coating; nanocomposite; co-electrodeposition; oxidation; hot corrosion

1 Introduction

Ni−Cr−Al coatings exhibit superior resistance against high temperature corrosion due to the selective oxidation of active elements to form thermodynamically stable and slowly growing protective oxides such as Cr_2O_3 and Al_2O_3 [1−5]. They can be used as the overlay coatings or as the bond coating of thermal barrier coatings (TBCs). Techniques applied to fabricate the Ni−Cr−Al coatings include magnetron sputtering [4], plasma spraying [5] and high velocity oxy-fuel spraying [6]. These coatings are highly alloyed and mainly composed of solid solutions or intermetallic compounds. The composite electrodeposition technique is a low-cost and low-temperature method suitable for producing metal matrix composite coatings with excellent properties for diverse purpose such as wear and abrasion resistance. In this process, fine particles or whiskers are suspended in the electrolyte and embedded in the growing metal layer. FOSTER et al [7] firstly prepared Ni−Cr−Al coatings by composite electrodeposition of Ni with pre-alloyed CrAlY microparticles. Unfortunately, the as-deposited coatings were not oxidation- and corrosion-resistant before heat pre-treatment. Recently, PENG et al [8−12] have developed novel Ni−Cr or Ni−Al nanocomposites by co-elecrodeposition of Ni with Cr or Al nanoparticles, respectively. For Ni−Al nanocomposite (Al particle size: 75 nm), the critical Al content to form alumina scale was about 13% [9]. For Ni−Cr nanocomposite (Cr particle size: 39 nm), the critical Cr content to form chromia scale was about 9.6% [11]. More recently, Ni−Cr−Al nanocomposites with dispersed Cr and Al nanoparticles have been produced [13,14]. The results indicated that the oxidation resistance of the Ni−Cr−Al nanocomposites profoundly depended on the total (Cr+Al) content, the Cr/Al ratio, and the actual Cr and Al particle size. At a given total (Cr+Al) content, the increase of Cr content significantly decreased the Al content to form alumina scale, a similar effect as the third element effect, which was first suggested by WAGNER [15]. Without heat pre-treatmet, Ni−6Cr−7Al nanocomposites exhibited a increased hot corrosion resistance than Ni−6Cr−7Al alloy under molten $(0.9Na, 0.1K)_2SO_4$ [14]. However, there is still no report about its hot corrosion under molten Na_2SO_4−NaCl salt. In this work, a Ni−7Cr−4Al nanocomposite was prepared through co- electrodeposition of Ni with Cr and Al nanoparticles, and its oxidation and hot corrosion under molten 75% Na_2SO_4 + 25% NaCl salts were investigated. For comparison, an electrodeposited Ni−11Cr nanocomposite and Ni-film were also performed

Foundation item: Project (11531319) supported by the Scientific Research Fund of Heilongjiang Provincial Education Department, China
Corresponding author: Hai-Jun ZHANG; Tel: +86-451-88036740: E-mail: zhj_7788@126.com
DOI: 10.1016/S1003-6326(15)63595-6

to elucidate the effect of Cr nanoparticles on the oxidation and hot corrosion of Ni−Cr−Al nanocomposite.

2 Experimental

Pure electrolytic nickel (>99.9% purity) specimens with dimensions of 15 mm × 10 mm × 2 mm were ground with 800-grit SiC paper, then were ultrasonically cleaned in acetone before co-electrodeposition. After being ultrasonically cleaned in acetone, they were electrodeposited (on all sides) with a 50−60 μm thick film of Ni−7Cr−4Al nanocomposite from a nickel sulfate bath containing 150 g/L $NiSO_4·7\ H_2O$, 15 g/L NH_4Cl, 15 g/L H_3BO_3, 0.1 g/L $C_{12}H_{25}NaSO_4$, and an appropriate content of Cr (average size: 40 nm) and Al (average size: 100 nm) nanoparticles. During electrodeposition, the nanoparticles were suspended in the bath by a reciprocating perforated plate [8−12]. The current density used was 3 A/dm^2, the temperature was 35 °C and the pH was 5.5−6.0. The nominal composition of the nanocomposite was Ni−7Cr−4Al. Its actual composition is presented in Table 1. For comparison, a 55 μm thick Ni−11Cr nanocomposite and Ni-film were also electroplated using the same electrolytic bath and the same parameters with and without Cr nanoparticles (average size: 40 nm). After the deposition, the as-deposited samples were rinsed by using distilled water and then ultrasonically cleaned for analysis.

Table 1 Actual compositions of nominal Ni−7Cr−4Al and Ni−11Cr nanocomposites based on EDS analysis

Sample	w(Cr)/%	w(Al)/%	w(Ni)/%
Ni−11Cr	11.3		Bal.
Ni−7Cr−4Al	7.2	4.2	Bal.

The isothermal oxidation experiments were carried out in air at 800 °C for 30 h. The hot corrosion test was carried out under molten 75% Na_2SO_4 + 25% NaCl salts in a muffle furnace in an ambient atmosphere at 750 °C, which is over the liquid temperature of ~620 °C for the mixed salt. Before exposure, specimens were preheated, followed by deposition with 1.6 mg/cm^2 salt film using hand-brushed techniques as provided elsewhere [7,8]. Then the specimens were placed in a crucible for hot corrosion testing. The specimens were taken out, cleaned, weighed and recoated with salt after certain time. The duration for the whole hot corrosion test was 30 h. The mass changes of the specimens were measured using an electrobalance with a detection limit of 0.01 mg. The films before and after oxidation and hot corrosion were analyzed by means of TECNAI-20 type transmission electron microscope (TEM), Camscan MX2600FE type scanning electron microscope/energy dispersive X-ray spectroscopy (SEM/EDS) and D/Max-2500 pc type X-ray diffraction (XRD). Electroless Ni-plating was plated on the surface of the oxidized specimens to prevent the spallation of the scales for observing cross-sections.

3 Results

3.1 Microstructure

A regular pyramidal structure is observed at the surface of the as-deposited nickel film due to a typical Ni growth texture [16]. With the addition of Cr nanoparticles, the morphology changes to nodular structure, as shown in Fig. 1. From the corresponding cross-section morphology shown in Fig. 2(a), it can be found that the black Cr nanoparticles are in general homogeneously dispersed in the Ni−Cr nanocomposite, although some of them form agglomerated clusters. However, with the addition of Cr and Al nanoparticles, a homogeneous dispersion of nanoparticles occurs, as seen in Fig. 2(b). The XRD patterns shown in Fig. 3 further confirmed the presence of Cr and Al nanoparticles in the Ni−Cr and Ni−Cr−Al nanocomposites. Figure 4 shows the bright-field TEM images of the light area of Ni−Cr and Ni−Cr−Al nanocomposites. The Cr and Al nanoparticles are uniformly dispersed in the nanocrystalline Ni matrix with the grain size of Ni ranging from 20 to 60 nm. No cracks and voids are observed in the nanocomposites.

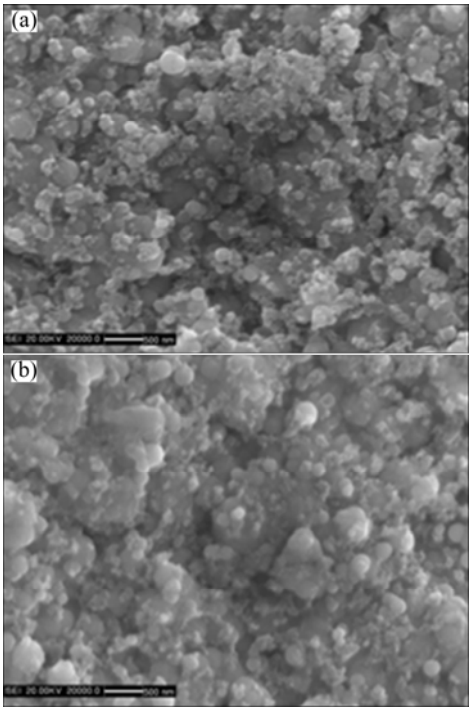

Fig. 1 Surface morphologies of as-deposited Ni−11Cr (a) and Ni−7Cr−4Al nanocomposite (b)

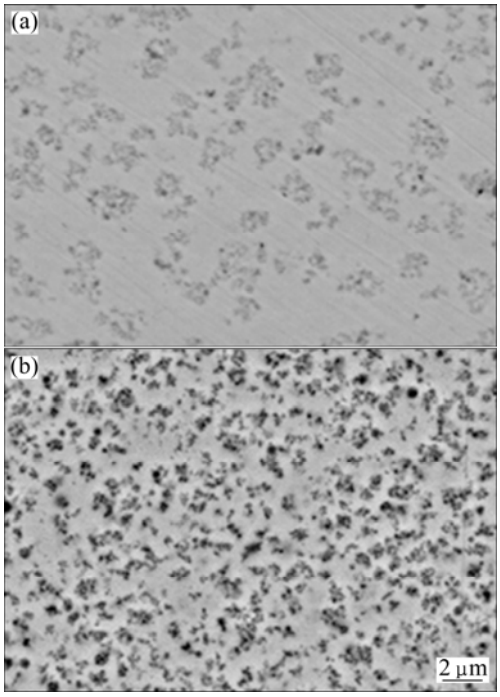

Fig. 2 Cross-sectional morphologies of as-deposited Ni−11Cr (a) and Ni−7Cr−4Al (b) nanocomposites

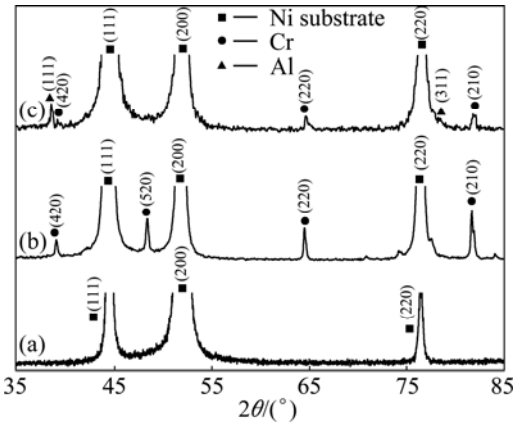

Fig. 3 XRD patterns of Ni-film (a), Ni−11Cr (b) and Ni−7Cr−4Al (c) nanocomposites

3.2 Oxidation resistance

Figure 5 shows the oxidation curves of the various samples in air at 800 °C for 30 h. During oxidation and cooling, no spallation occurs for the three samples. Clearly, both Ni−11Cr and Ni−7Cr−4Al nanocomposites exhibit a lower scaling rate in the first 5 h, especially the Ni−7Cr−4Al nano composites. In this stage, a continuous protective scale is expected to have been thermally grown. After this period, a significant mass gain occurs for Ni-film. However, the oxidation rates of the Ni−11Cr and Ni−7Cr−4Al nanocomposite maintain so low that no significant mass gain occurs. These indicate that Ni−11Cr exhibits better oxidation resistance than Ni-film. However, Ni−7Cr−4Al with lower Cr content and minor

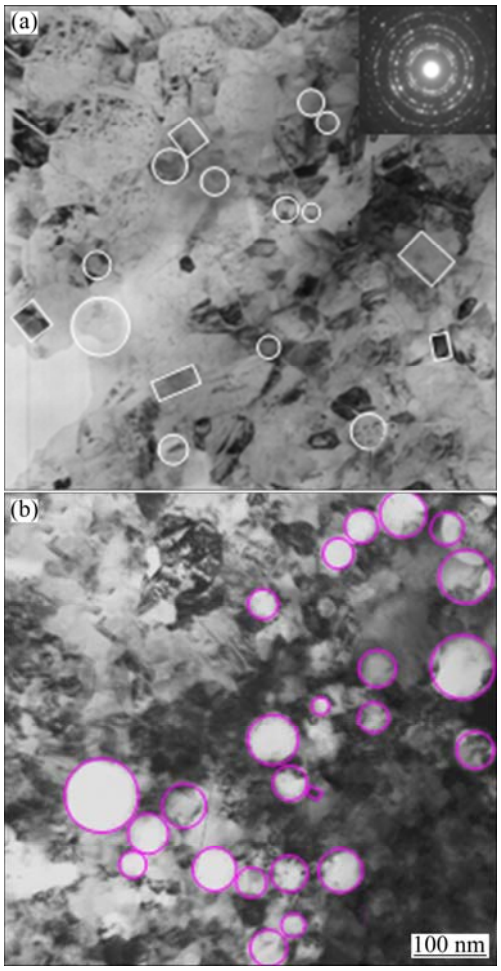

Fig. 4 TEM bright-field images of as-deposited Ni−11Cr (a) and Ni−7Cr−4Al (b) nanocomposites

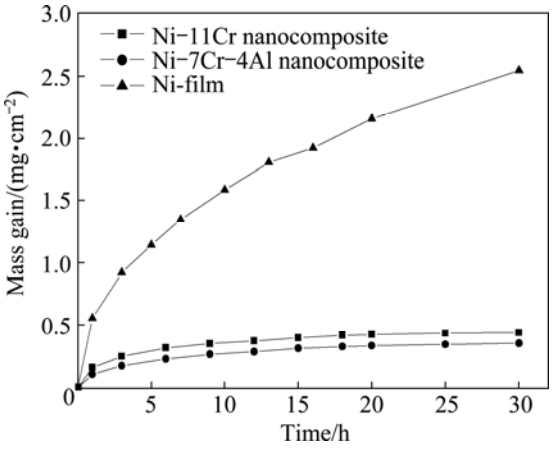

Fig. 5 Oxidation kinetics of various samples at 800 °C for 30 h

Al exhibits better oxidation resistance than Ni−11Cr nanocomposite.

The oxides formed are characterized using XRD. Only NiO forms on Ni-film [17]. The scale formed on the Ni−11Cr consists of major Cr_2O_3 and minor $NiCr_2O_4$ and NiO, while the scale formed on the Ni−7Cr−4Al nanocomposite consists of major Al_2O_3 and minor

$Ni(Al,Cr)_2O_4$ and NiO scale, as shown in Fig. 6. In addition, the peak intensities of substrate on Ni−7Cr−4Al nanocomposite are much stronger than those on Ni−11Cr nanocomposite, which suggests the formation of a thinner scale on Ni−7Cr−4Al nanocomposite.

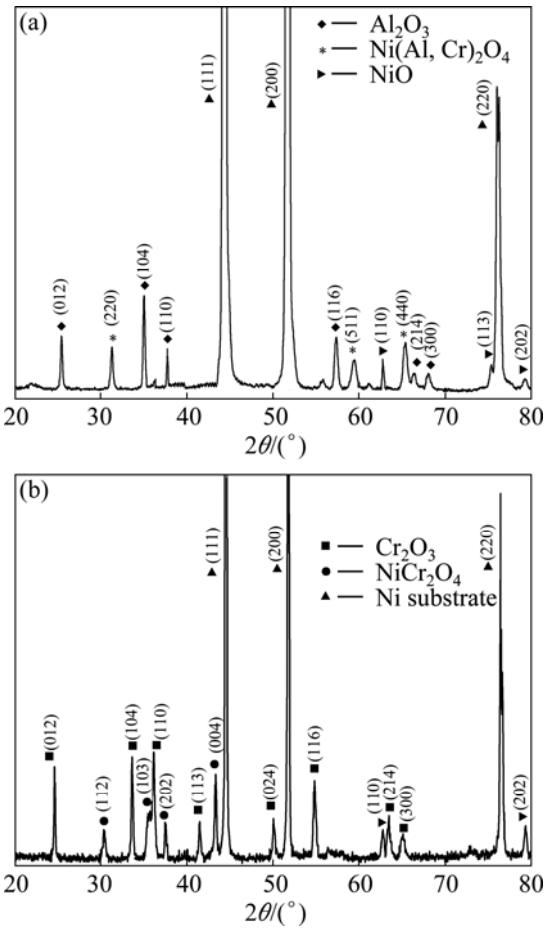

Fig. 6 XRD patterns of scales on Ni−11Cr (a) and Ni−7Cr−4Al (b) nanocomposites exposed in air at 800 °C for 30 h

Faceted NiO grains with average size of 7.5 μm form on the Ni-film after 30 h oxidation at 800 °C [17]. However, for the Ni−11Cr and Ni−7Cr−4Al nanocomposites, significantly fine oxide appears, as shown in Figs. 7(a) and (b), respectively. Typical faceted and small-grained crystals with average size of 1.5 μm are observed on the oxidized Ni−11Cr nanocomposite. EDS results indicate that the oxide is rich in Cr. In contrast, most of oxides formed on Ni−7Cr−4Al nanocomposite are so fine that their crystal shape is difficult to inspect. EDS results indicate that the small faceted grain is rich in Cr, and the oxides on other area are rich in Al. Based on the EDS and XRD results, it can be concluded that the small faceted grain may be Cr_2O_3, however, the oxides on the other area are Al-rich oxide (Al_2O_3 or Ni (Al, Cr) $_2O_4$ spinel). These results suggest that Ni−11Cr nanocomposite forms chromia scale, but Ni−7Cr−4Al nanocomposite forms alumina scale.

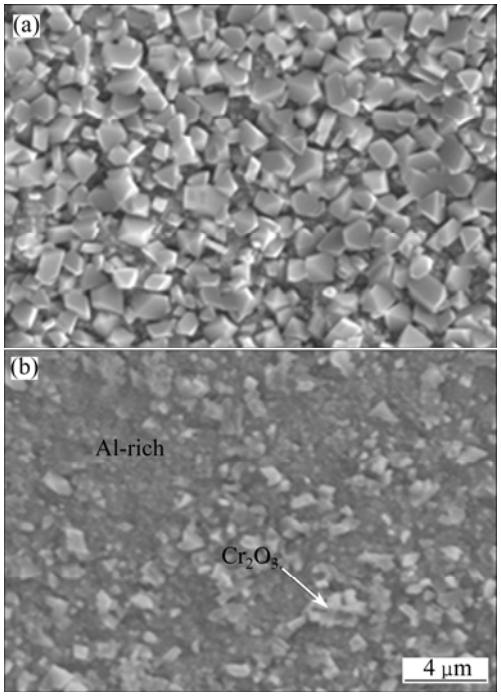

Fig. 7 Surface morphologies of oxides scales formed on Ni−11Cr (a) and Ni−7Cr−4Al (b) nanocomposites at 800 °C for 30 h

Figure 8 presents the corresponding cross-sectional morphologies of the oxide scale. It is clear that a thinner scale forms on Ni−7Cr−4Al nanocomposites. The original nanoparticles, as seen in the BEI in Fig. 2, disappear in the nanocomposites even deeply below the scale. At the same time, micro-voids form as a result of the annealing-related volume shrinkage [18−20].

3.3 Hot corrosion resistance

Figure 9 illustrates the hot corrosion kinetics of various samples in air at 750 °C under molten 75% Na_2SO_4 + 25%NaCl salts. Ni-film is corroded very quickly during the first 5 h of exposure. Compared to Ni-film, the hot corrosion of the Ni−11Cr and Ni−7Cr−4Al nanocomposites is not significant. Compared to the Ni−11Cr nanocomposite, Ni−7Cr−4Al nanocomposite exhibits much lower scaling rate and higher hot corrosion resistance.

After hot corrosion, the oxide formed is characterized using XRD, as seen in Fig. 10. Only NiO forms on Ni-film. The scales formed on the Ni−11Cr and Ni−7Cr−4Al nanocomposites consist of major Cr_2O_3 and minor NiO and $NiCr_2O_4$. In the meantime, stronger peaks of chromate (Na_2CrO_4) are seen as a result of the preferential reaction of chromia with oxides in the molten salt.

Figure 11 presents the cross-sections of various samples after hot corrosion. Severe scale cracking and separation between the scale and the metal occur on

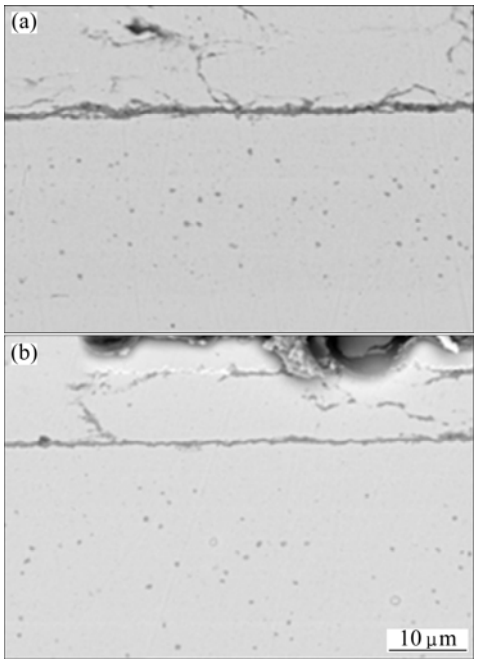

Fig. 8 Cross-sectional morphologies of oxide scales formed on Ni−11Cr (a) and Ni−7Cr−4Al (b) nanocomposites at 800 °C for 30 h

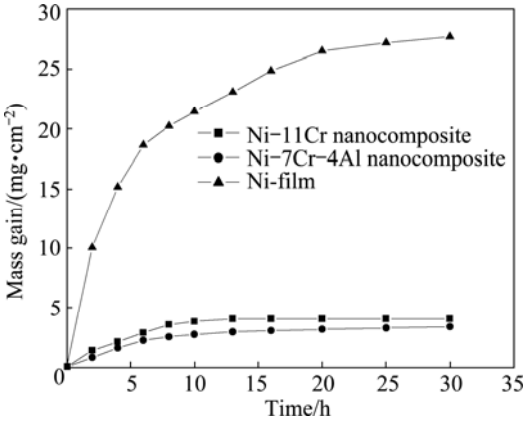

Fig. 9 Mass change vs time curves of various samples exposed in air at 750 °C for 30 h under molten salt of 75% Na_2SO_4+ 25% NaCl

the Ni-film (Fig. 11(a)). For Ni−11Cr nanocomposite, a thinner chromia scale with cracking and significant internal corrosion occurs. The internal corrosion products are sulfides. In contrast, for Ni−7Cr−4Al nanocomposite, an inner Al-richen layer below outer chromia scale occurs locally with slight internal corrosion.

4 Discussion

4.1 Oxidation resistance

Previous investigations [11,12] showed that Ni−Cr nanocomposites with different Cr contents can develop different scales as addressed below. When oxidation starts, NiO and Cr_2O_3 simultaneously nucleate,

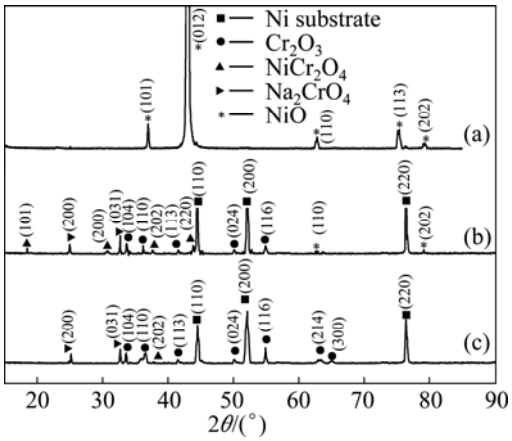

Fig. 10 XRD patterns of scales formed on Ni-film (a), Ni−11Cr (b) and Ni−7Cr−4Al (c) nanocomposites exposed in air at 750 °C for 30 h under molten salt of 75% Na_2SO_4 + 25% NaCl

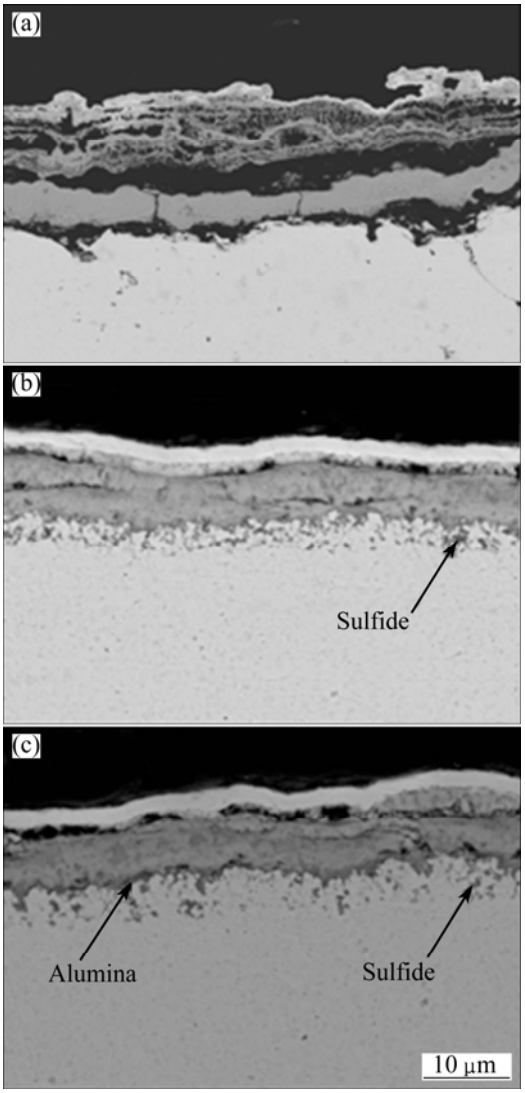

Fig. 11 Cross-sectional morphologies of oxide scales formed on Ni-film (a), Ni−11Cr (b) and Ni−7Cr−4Al (c) nanocomposites under molten salt of 75% Na_2SO_4+25% NaCl in air at 750 °C for 30 h

respectively, on the nanocrystalline Ni and on the Cr nanoparticles. After that, the thickening of NiO and lateral coalescing of the Cr_2O_3 islands begin. If the Cr content is lower than the critical content to form continuous chromia scale, NiO grows rapidly and engulfs the Cr_2O_3 islands. In this case, the nano composite exhibits a higher oxidation rate than Ni-film. Conversely, if the Cr content exceeds the critical content, the initially formed Cr_2O_3 islands can link together through their lateral growth during a short initial stage to form a continuous chromia layer. This is why Ni−11Cr nanocomposite exhibits better oxidation resistance than Ni-film.

For Ni−7Cr−4Al nanocomposite, Al_2O_3 also nucleates on Al nanoparticles simultaneously. Then Cr_2O_3 and Al_2O_3 islands can link together through their lateral growth during a short initial stage to form a continuous and mixed Cr_2O_3 and Al_2O_3 layer. The formation of mixed layer efficiently suppresses the NiO growth. After that, its thickening starts. Because Cr_2O_3 and Al_2O_3 can form continuous solid solutions $(Cr_{1-x}Al_x)_2O_3$ [21,22] due to a similar corundum, hexagonal close-packed (HCP) crystal structure, $(Cr_{1-x}Al_x)_2O_3$ scale will form. But with the oxidation, the larger Al flux in comparison to the Cr flux will convert the Al-rich layer into an Al_2O_3 layer. This is why Ni−7Cr−4Al nanocomposite with lower Cr and minor Al can form an alumina scale and exhibit better oxidation resistance than Ni−11Cr nanocomposite. In long time, the reaction of NiO with Cr_2O_3 and Al_2O_3 will cause the formation of $Ni(Al,Cr)_2O_4$.

4.2 Hot corrosion

According to GOEBEL et al [23,24] and RAPP et al [25,26], materials may be attacked through the following route: the molten salt penetrates the growing oxide scale through defects like pores and microcracks and arrives at the scale/alloy interface, SO_4^{2-} is then reduced there by the following chemical reaction:

$$2SO_4^{2-}=2O^{2-}+3O_2+2S \quad (1)$$

This leads to the internal sulfidation of the materials [27]. Internal sulfidation causes a reduction of S activity and, as a result, an increase of O^{2-} activity, resulting in basic fluxing of oxide scale. As a negative gradient of the O^{2-} activity exists across the fused salt layer, the dissolution of oxide scale at the salt/scale interface and the reprecipitation of oxide particles at the gas/salt interface can be sustained. For Ni-film, surface NiO layer normally forms at the onset of exposure. The defects in NiO layer make it feasible that the molten salt penetrates into the internal interface, where the increase of O^{2-} activity by Reaction (1) will dissolve the oxide by the reaction below [12,14]:

$$NiO+O^{2-}=NiO_2^{2-} \quad (2)$$

Reaction (2) again decreases the O^{2-} activity, which further increases the S activity. In this case, the alloy is repeatedly attacked by sulfur and a thicker scale forms, as shown in Fig. 11(a).

For Ni−11Cr nanocomposites, it can grow a chromia scale in a short transient oxidation stage. Chromia is the most important oxide to combat hot corrosion in molten salt with sulfates, because it preferentially reacts with O^{2-} in molten sulfates to form chromate by the following reaction [23−26]:

$$2Cr_2O_3+4O^{2-}+3O_2=4CrO_4^{2-} \quad (3)$$

The chromate will stabilize the melt chemistry, and consequently prevent the dissolution/reprecipitation of the protective oxide scale, thus less internal sulfide occurs, as seen in Fig. 11(b). However, for Ni−7Cr−4Al nanocomposite, less internal sulfides and better hot corrosion resistance are observed. This is possibly associated with two factors. First, the compact protective chromia scale fast forms. Second, Al-rich oxides formed below the Cr-rich oxides layer (see Fig. 11(c)) further prevents the penetration of salts into the scale/nanocomposite interface. To confirm this assumption, a comparison of initial scale on both nanocomposites for 1 h exposure in the hot corrosion condition was performed. As is evident from Fig. 12, a more compact scale forms on Ni−7Cr−4Al nanocomposite. Cross-sectional mophologies also reveal that local alumia oxides below outer chromia form on Ni−7Cr−4Al nanocomposite, as seen in Fig. 13(b).

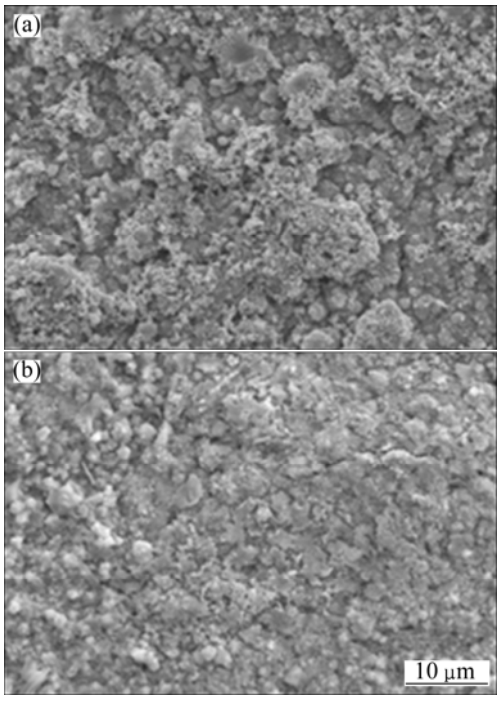

Fig. 12 Surface morphologies of oxides scale formed on Ni−11Cr (a) and Ni−7Cr−4Al (b) nanocomposites under molten salt in air at 750 °C for 1 h

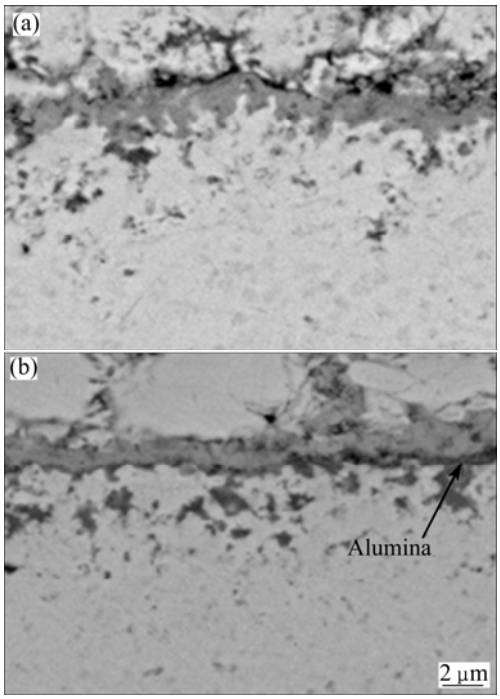

Fig. 13 Cross-sectional morphologies of oxides scale formed on Ni−11Cr (a) and Ni−7Cr−4Al (b) nanocomposites under molten salt in air at 750 °C for 1 h

5 Conclusions

1) Ni−Cr−Al nanocomposites with nanocrystalline Ni grain could be fabricated through coelectrodeposition of Ni with Cr and Al nanoparticles.

2) Compared with Ni−11Cr nanocomposite and Ni-film, Ni−7Cr−4Al nanocomposite exhibits a dramatically high oxidation resistance because Cr_2O_3 nuclei formed on Cr nanoparticles act as Al_2O_3 nuclei, which significantly decrease the Al content to form alumina scale and promote the fast formation of alumina scale.

3) The formation of local Al_2O_3 oxides below outer Cr_2O_3 layer improves the hot corrosion resistance of Ni−7Cr−4Al nanocomposite under molten 75% Na_2SO_4+ 25% NaCl salts.

References

[1] TAWANCY H M, ABBAS N M, BENNETT A. Role of Y during high temperature oxidation of an M−Cr−Al−Y coating on an Ni-base superalloy [J]. Surface and Coatings Technology, 1994, 68−69: 10−16.

[2] LIU Z Y, GAO W. Oxidation behaviour of microcrystalline Ni−Cr−Al alloy coatings at 900 °C [J]. Scripta Materialia, 1998, 38(6): 877−885.

[3] XU C Z, JIAG S M, BAO Z B, GONG J, SUN C. Isothermal oxidation behaviour of a gradient NiCoCrAlSiY coating deposited by arc ion plating on a Ni-based single crystal superalloy [J]. Corrosion Science, 2009, 51(6): 1467−1474.

[4] LI Q, PENG X, ZHANG J Q, ZONG G X, WANG F H. Comparison of the oxidation of high-sulfur Ni−25Cr−5Al alloys in as-cast and as-sputtered states [J]. Corrosion Science, 2010, 52(4): 1213−1221.

[5] WEI Qi, YIN Zhi-yong, LI Hui. Oxidation control in plasma spraying NiCrCoAlY coating [J]. Applied Surface Science, 2012, 258(12): 5094−5099.

[6] ZHAO L D, PARCO M, LUGSCHEIDER E. High velocity oxy-fuel thermal spraying of a NiCoCrAlY alloy [J]. Surface and Coatings Technology, 2004, 179(2): 272−278.

[7] FOSTER J, CAMERON B P, CAREW J A. The production of multi-component alloys coatings by particle codeposition [J]. Trans Inst Met Finish, 1985, 63(3−4): 115−119.

[8] ZHOU Y, PENG X, WANG F. Oxidation of a novel electrodeposited Ni−Al nanocomposite film at 1050 °C [J]. Scripta Materialia, 2004, 50(12): 1429−1433.

[9] ZHOU Y, PENG X, WANG F. Size effect of Al particles on the oxidation of electrodeposited Ni−Al composite coatings [J]. Oxidation of Metals, 2005, 64(3−4): 169−183.

[10] ZHOU Y**,** PENG X, WANG F. Cyclic oxidation of alumina-forming Ni−Al nanocomposites with and without CeO_2 addition [J]. Scripta Materialia, 2006, 55(11): 1039−1042.

[11] ZHANG Y, PENG X, WANG F. Development and oxidation at 800 °C of a novel electrodeposited Ni−Cr nanocomposite film [J]. Materials Letters, 2004, 58(6): 1134−1138.

[12] ZHANG C, PENG X, ZHAO J, WANG F. Hot corrosion of an electrodeposited Ni−11wt%Cr nanocomposite under molten Na_2SO_4–K_2SO_4−NaCl [J]. Journal of the Electrochemical Society B, 2005, 152 (9): 321−326.

[13] YANG X, PENG X, XU C, WANG F. Electrochemical assembly of Ni–*x*Cr–*y*Al nanocomposites with excellent high-temperature oxidation resistance [J]. Journal of the Electrochemical Society C, 2009, 156(5): 167−175.

[14] YANG X, PENG X, WANG F. Hot corrosion of a novel electrodeposited Ni−6Cr−7Al nanocomposite under molten $(0.9Na,0.1K)_2SO_4$ at 900 °C [J]. Scripta Materialia, 2007, 56(10): 891−894.

[15] WAGNER C. Passivity and inhibition during the oxidation of metals at elevated temperatures [J]. Corrosion Science, 1965, 5(11): 751−764.

[16] ZHOU Y B, QIAN B Y, ZHANG H J. Al particles size effect on the microstructure of the co-deposited Ni−Al composite coatings [J]. Thin Solid Films, 2009, 517(11): 3287−3291.

[17] ZHANG Hai-jun, ZHOU Yue-bo, SUN Jian-feng. Preparation and oxidation behaviour of electrodeposited Ni−CeO_2 nanocomposite coatings [J]. Transactions of Nonferrous Metals Society of China, 2013, 23(7): 2011−2020.

[18] DONG Z, PENG X, GUAN Y, LI L, WANG F. Optimization of composition and structure of electrodeposited Ni−Cr composites for increasing the oxidation resistance [J]. Corrosion Science, 2012, 62: 147−152.

[19] PENG X, LI M, WANG F. A novel ultrafine-grained Ni_3Al with increased cyclic oxidation resistance [J]. Corrosion Science, 2011, 53(4): 1616−1620.

[20] ZHOU Yue-bo, ZHANG Hai-jun. Effect of annealing treatment on cyclic-oxidation of electrodeposited Ni−Al nanocomposite [J]. Transactions of Nonferrous Metals Society of China, 2011, 21(2): 322−329.

[21] JACOB K T. Electrochemical determination of activities in Cr_2O_3−Al_2O_3 solid solution [J]. Journal of the Electrochemical Society, 1978, 125: 175−179.

[22] KIM S S, SANDERS T H. Thermodynamic modeling of the isomorphous phase diagrams in the Al_2O_3−Cr_2O_3 and V_2O_3−Cr_2O_3 systems [J]. Journal of the American Ceramic Society, 2001, 84: 1881−1884.

[23] GOEBEL J A, PETTIT F S. Na_2SO_4-induced accelerated oxidation of

nickel [J]. Metallurgical and Materials Transactions B, 1970, 1: 1943−1954.

[24] GOEBEL J A, PETTIT F S, GOWARD G. W. Mechanisms for the hot corrosion of nickel-based alloy [J]. Metallurgical and Materials Transactions B, 1973, 4: 261−278.

[25] GUPTA D K, RAPP R A. The solubilities of NiO Co_3O_4 and ternary oxides in fused Na_2SO_4 at 1200 K [J]. Journal of the Electrochemical Society, 1980, 127: 2194−2202.

[26] ZHANG Y S, RAPP R A. Solubilities of α-Fe_2O_3 and Fe_3O_4 in fused Na_2SO_4 at 1200 K [J]. Journal of the Electrochemical Society, 1985, 132: 2498−2501.

[27] LI M H, SUN X F, HU W Y, GUAN H G, CHEN S G. Hot corrosion of a single crystal-Ni-base superalloy by Na-salts at 900 °C [J]. Oxidation of Metals, 2006, 65(1−2): 137−150.

Ni−7Cr−4Al 纳米复合镀层的氧化和热腐蚀性能

张海军，孙俭峰

黑龙江科技大学 材料科学与工程学院，哈尔滨 150022

摘　要：采用复合电镀技术，通过向普通硫酸镍电镀液中加入纳米 Cr 和 Al 颗粒，在 Ni 基材上制备了一种 Ni−7Cr−4Al (质量分数，%)纳米复合涂层，对其在 800 °C 下的空气氧化和 750 °C 下 75% Na_2SO_4+25% NaCl 混合熔盐热腐蚀性能进行研究。作为对比，对相同工艺制备的 Ni−11Cr 纳米复合镀层和纯 Ni 镀层的氧化和热腐蚀性能进行分析。Cr 和 Al 纳米颗粒弥散分布在 20~60 nm 的纳米 Ni 中，与 Ni−11Cr 纳米复合镀层和纯 Ni 镀层相比，Ni−7Cr−4Al 纳米复合镀层由于能快速形成氧化铝膜而表现出更优异的抗氧化性能，同时氧化铝膜的快速形成也提高了涂层的热腐蚀性能。

关键词：Ni−Cr−Al 涂层；纳米复合物；复合电镀；氧化；热腐蚀

(Edited by Yun-bin HE)